Lifetime and mean free path of spin waves in ultrathin cobalt films

E. Michel,[1,2] H. Ibach,[2,3,*] C. M. Schneider,[1,2] D. L. R. Santos,[4,†] and A. T. Costa[5]
[1]*Peter Grünberg Institut (PGI-6), Forschungszentrum Jülich, 52425 Jülich, Germany*
[2]*Jülich Aachen Research Alliance, Germany*
[3]*Peter Grünberg Institut (PGI-3), Forschungszentrum Jülich, 52425 Jülich, Germany*
[4]*Laboratoire Louis Néel, CNRS, Boite Postale 166, 38042 Grenoble Cedex 09, France*
[5]*Instituto de Física, Universidade Federal Fluminense, 24210-346 Niterói, R. J., Brazil*
(Received 6 November 2015; revised manuscript received 30 May 2016; published 18 July 2016)

Miniaturization of magnon-based devices into the nanometer range would require the utilization of exchange-dominated spin waves of nanometer wavelength. In experiment and theory we show that the intrinsic lifetime and mean free path of the homogeneous acoustic spin wave in ultrathin cobalt films is sufficiently long for such applications provided that the films are atomically flat. The presence of surface steps, however, shortens lifetime and mean free path. The experimental data are consistent with a model which assumes that steps act as perfect sinks for spin waves.

DOI: 10.1103/PhysRevB.94.014420

I. INTRODUCTION

The utilization of magnons (spin waves) is one of the prime topics on the magnetism road map [1]. The field is commonly addressed as "magnonics." Special interest has been devoted to magnon-based devices for data buffering and logic gates, and demonstrators have been proposed and realized [2–4]. Magnon-based devices require a long lifetime of magnons, which so far has been realized primarily in yttrium iron garnet (YIG) and permalloy [2,5], and only for magnon wavelengths in the micrometer range. The miniaturization of magnon-based devices into the nanometer (nm) range and the extension into a higher frequency range would require the employment of exchange-dominated high frequency spin waves of nm wavelength.

High frequencies, high group velocities, and wavelengths in the sub-nm range are realized by acoustic ferromagnetic spin waves in ultrathin 3*d*-metal films. These spin waves have been explored experimentally in the last decade using inelastic scattering of low energy electrons [6–9]. Because of limitations in the energy resolution the experimental database was confined to wave vectors between about 3 nm^{-1} and the boundary of the surface Brillouin zone. In that range, the lifetime of spin waves is extremely short (<100 fs) [10,11]. The reason for the short lifetime is the abundance of decay channels into electron-hole spin-flip excitations (Stoner excitation). Correspondingly, the mean free path of a spin wave packet (defined as the product of group velocity and lifetime) is only of the order of 1 nm. These modes are therefore not suitable for technical applications.

Theoretical studies of acoustic thin film modes with smaller wave vectors (smaller than hitherto accessible by inelastic electron scattering) show however that spin waves of sufficiently long lifetimes should exist even in 3*d* metals [12–17]. For an eight atom layer cobalt film epitaxially grown on Cu(100) and a wave vector $q = 1$ nm^{-1}, e.g., our theory (see below) predicts a lifetime $\tau = 12$ ps, a frequency 1 THz ($\hbar\omega = 4$ meV), and a mean free path of 150 nm. Theory predicts furthermore that the lifetime increases proportional to q^{-4} [14]. Spin waves of this type may therefore suit to carry magnonics into the size scale of nanometers.

In this paper we report on high resolution data of acoustic spin waves in ultrathin fcc cobalt layers deposited on Cu(100) surfaces. The results are compared to a theory of spin excitations which takes into account the itinerant character of the electrons. For eight atom layer (8 ML) films with a small density of surface steps and wave vectors $q < 2$ nm^{-1} we find indeed that the intrinsic full width at half maximum (FWHM) is below 1 meV, corresponding to a lifetime of several picoseconds, in agreement with our theory. However, those sharp spin wave spectra are observed only for well-annealed films with a small density of surface steps. Spin waves of films in their as-grown state with a higher step density display considerably larger FWHM, far above the theoretical values. We demonstrate that the results are consistent with the assumption that steps crossing the path of spin waves limit their mean free path. This understanding is corroborated by results on spin waves of cobalt films deposited on a Cu(1 1 23) surface. These films feature a regular array of oriented one-atom-high steps. We show that spin waves propagating parallel to the steps remain unaffected by the steps while perpendicular to the propagation path the spin waves are damped to the extent that they cease to exist as defined excitations. We conclude that for small wave vectors the lifetime of spin waves in ultrathin 3*d*-metal films is primarily determined by the density and orientation of one-atom-high steps, rather than by intrinsic properties of the material.

The paper is organized as follows. The next section is devoted to experimental results. It demonstrates the capability of our present electron energy loss spectrometer, shows raw data for the full width at half maximum (FWHM) of the spin wave signals, and describes the correlation of the results with the magnitude of the elastic diffuse scattering. The latter data are simulated by a model involving a random array of steps of variable density. Section III describes the procedure by which the intrinsic FWHM is extracted from the data by making use of the known momentum and energy resolution functions of the spectrometer. Section IV is devoted to the theoretical

*h.ibach@fz-juelich.de
†On sabbatical leave from Centro Federal de Educação Tecnológica, Itagaí 23812-101, Rio de Janeiro, Brazil.

approach by which we determine energy and FWHM of the acoustic spin waves. Section V discusses the intrinsic lifetime of spin waves for wave vectors between 1 and 3 nm^{-1} and compares our results in experiment and theory to previous studies for larger wave vectors. In Sec. VI the mean free path of spin waves is calculated from the experimental data and the result is compared to a model which assumes that steps crossing the path of spin waves act as complete sinks for those spin waves. Conclusions are presented in Sec. VII.

II. EXPERIMENT

Our experiments concern epitaxial cobalt films deposited on Cu(100) substrates at room temperature. These films nucleate via homogeneous nucleation and grow as pseudomorphic fcc films in the Frank–van der Merwe growth mode [18,19]. This growth mode is frequently called "layer-by-layer growth." However, even in the ideal case the film thickness is not uniform but varies in height by ±1 layer (see, e.g., Chap. 11 of [20]). The film surface therefore displays monolayer high islands and vacancy islands. The average size of these islands and therefore the density of one-atom layer high steps on the surface depends on the diffusion constant of cobalt on the copper surface, the interlayer diffusion on the growing cobalt film, and the evaporation flux; the faster the diffusion and the lower the evaporation flux the lower is the density of steps [20]. Low step densities could therefore be achieved by raising the deposition temperature. In the case of cobalt on copper, however, higher deposition temperatures lead to intermixing at the cobalt-copper interface. A reduction of the density of surface steps without causing intermixing is possible by moderate annealing to temperatures up to 450 K. At this temperature the interlayer diffusion of cobalt atoms across steps is large enough to initiate smoothening of the surface and thereby a reduction of the density of surface steps. A prerequisite for the realization of the scenario described above is that the surface is free of contaminants since contaminants act as nucleation centers and hinder the free flow of steps by pinning the steps at those impurities. Our films are prepared by *e*-beam assisted evaporation from a cobalt rod. The film thickness is calibrated vs the ion current of the evaporator via the oscillations in the intensity of reflected 3 keV electrons at grazing incidence ("MEED oscillations") [8,21,22]. Low contamination levels of the films of less than 10^{-4} of a monolayer [21] are ensured by heating the cobalt rod in a quartz furnace to 1300 °C in an $\mathrm{Ar}:\mathrm{H}_2$ atmosphere for 24 h prior to mounting in the evaporator. Careful outgassing of the evaporator and a low pressure ($<10^{-10}$ mbar) during evaporation is likewise required.

The electron energy loss spectrometer used in this study is of the type described in Refs. [23,24], however equipped with a new, more compact electron emission system. About seven times higher currents are thereby achieved, which allows for an increase in resolution by a factor of 2 without loss of count rate. In the interest of a good signal-to-noise ratio required for unfolding the spectra we operate the spectrometer at 3.5 meV resolution in the low wave vector range ($q_{||} < 2.5\ \mathrm{nm}^{-1}$) and at 6 meV for larger wave vectors. Electron impact energies are $E_0 = 2.25\,\mathrm{eV}$ and $E_0 = 6\,\mathrm{eV}$ for 3.5 and 6 meV resolution spectra, respectively. The wave vector parallel to the surface

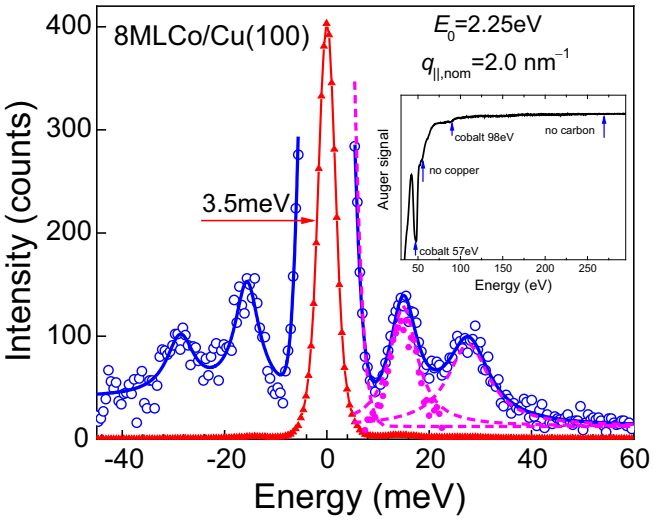

FIG. 1. Spin wave spectrum of an annealed 8 ML fcc cobalt film deposited on Cu(100). The elastic diffuse line (red triangles) shows the resolution of 3.5 meV FWHM. Spectra on the energy loss and energy gain side are corrected for the Bose-occupation number. The solid blue line is a fit by a Gaussian for the tail and two Lorentzians riding on small background. The resulting individual contributions to the total fit are plotted as magenta colored dashed lines. The inset shows the low-energy Auger spectrum taken after annealing.

$q_{||}$ is determined by making use of wave vector conservation which for an energy loss reads

$$q_{||} = k^{(\mathrm{f})} \sin(\theta^{(\mathrm{f})}) - k^{(\mathrm{i})} \sin(\theta^{(\mathrm{i})}). \quad (1)$$

Here $k^{(\mathrm{i})}$ and $k^{(\mathrm{f})}$ are the moduli of k vectors of the incident and scattered electron, respectively, and $\theta^{(\mathrm{i})}$ and $\theta^{(\mathrm{f})}$ are the angles with respect to the normal of the surface. The desired wave vector of the spin wave parallel to surface is chosen by rotation of the sample around the axis vertical to the scattering plane. Spectra are recorded at a fixed rotation angle. Since the electron impact energy is relatively low the true wave vector varies slightly with the magnitude of the energy loss. For example, for $E_0 = 2.25\,\mathrm{eV}$, a nominal $q_{||} = 2\,\mathrm{nm}^{-1}$, and an energy loss of 15 meV, the true wave vector is $1.97\,\mathrm{nm}^{-1}$.

A sample spectrum of an eight atom layer (8 ML) cobalt film is shown in Fig. 1. The film is grown at room temperature and annealed afterwards to about 450 K for 30 min. The wave vector parallel to the surface $q_{||}$ is oriented along the [110] ($\bar{\Gamma}\bar{X}$) direction. Data accumulation time was 3 s/channel. The energy losses on the right and left side of the elastic peak are energy loss and gain due to the acoustic mode at ∼15 meV and the first standing mode of the film at ∼28 meV. This standing mode has a node in the precession amplitude situated near the center of the film. The intensity of standing modes with more than one or two nodes is suppressed in an energy loss spectrum, primarily because the spin wave amplitude oscillates as a function of the layer number and the contributions of individual layers cancel therefore [7,22].

The standing mode frequency depends critically on the film thickness [7]. The sharpness of the standing mode in Fig. 1 therefore excludes any significant intermixing and roughening at the interface due to the annealing process. The low energy Auger spectrum (inset in Fig. 1) shows furthermore that no

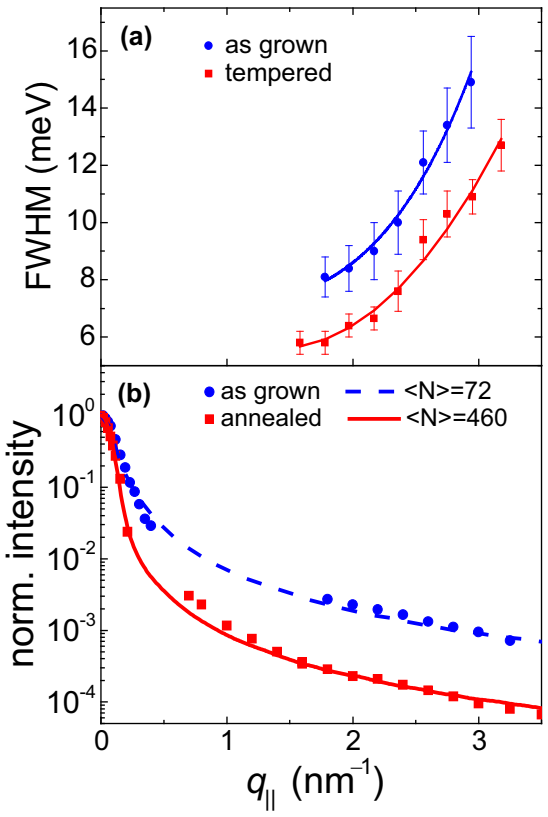

FIG. 2. (a) FWHM of the acoustic spin wave signal on an 8 ML cobalt film on a Cu(100) substrate before and after annealing as function of $q_{||}$ (blue circles and red squares, respectively). (b) Normalized intensity of the elastic peak vs $q_{||}$ before and after annealing (blue circles and red squares, respectively). All data stem from the same film. The solid line is the result of a simulation (see text).

significant amount of copper has crept to the surface, an effect commonly observed after heating to higher temperatures or heating for prolonged times [25].

The FWHM of the acoustic spin wave signal is extracted by first fitting the spectra on the energy loss side by a Gaussian for the tail and two Lorentzians riding on a small background (solid blue line in Fig. 1). The resulting individual contributions to the total fit are plotted as magenta colored dashed lines. Using the described procedure we have extracted the FWHM of the acoustic spin wave signals from experimental spectra between 1.6 and 3 nm^{-1} before and after annealing of the films. Figure 2(a) shows the result of one series of experiments obtained on the same film before and after annealing. The lower wave vector limit results from the fact that energy loss merges with the tail of the instrumental energy resolution function. The upper wave vector limit is owed to the merging of acoustic and standing wave signals at higher $q_{||}$. The results show that the process of annealing leads to a considerable reduction in the FWHM of the spin waves.

In order to understand and analyze quantitatively the effect of annealing we have measured the elastic diffuse intensity which is a measure of the crystalline order of the films. Figure 2(b) shows the normalized intensity of the elastic peak in the spectra, hence the elastic diffuse scattering, as function of wave vector $q_{||}$. Data at small $q_{||}$ are obtained by measuring the reflected current using a picoamperemeter. Data at higher $q_{||}$ are taken from the count rates of the elastic peaks in energy loss spectra. The gap between the data points obtained by direct measurement of the current and in the electron count mode is due to the gap between the lower limit of direct current measurements and the upper limit of the channeltron count rate. We emphasize that all data stem from the same film so that spectra and diffuse elastic intensity are directly correlated.

Elastic scattering outside the specular reflected beam at $q_{||} = 0$ is caused by defects. At the low impact energies used here the specular reflection is almost entirely due to the surface barrier. Hence the diffuse scattering must also result from a roughness of that barrier. The principle candidates for the roughness are impurity atoms on the surface (which do not necessarily coalesce) and the aforementioned steps generated in the growth process. Because of the low contamination level of our films impurities are excluded which leaves the one-atom-high steps as the remaining cause for the diffuse scattering. This understanding is corroborated by the large reduction in the intensity of the diffuse scattering upon annealing of the sample since annealing reduces the step density (see above).

Further support is obtained from a theoretical study of the elastic diffuse surface scattering of stepped surfaces. The solid lines in Fig. 2(b) are the result of a calculation of the elastic surface scattering from a (100) surface with a random distribution of up and down steps. The assumed mean terrace widths are 72 atom lengths, equivalent to 18.5 nm, and 460 atom lengths, equivalent to 118 nm for the annealed surface. The theoretical result matches the experimental data in the entire momentum range.

The experimental results so far prove that the presence of steps on a surface causes an increase of the FWHM of spin waves. In the following we show that steps affect spin waves primarily when the steps cross the path of spin wave, hence when the wave vector is oriented perpendicular to the steps. For that purpose we have studied spin wave spectra of an 8 ML cobalt film deposited on Cu(1 1 23). Figure 3(a) shows the LEED pattern of the 8 ML Co film on Cu(1 1 23) substrate at 142 eV electron energy. The pattern displays the characteristic spot splitting due to destructive interference of electrons scattered from different terraces. The splitting into two spots rather than into streaks proves a narrow terrace-width distribution, which is in agreement with STM images [26]. Figure 3(b) shows a kinematic simulation of the pattern of an ideal fcc cobalt film on (1 1 23) surface. Spin wave spectra for wave vectors oriented parallel and perpendicular to the steps are obtained by rotating the crystal *in situ* with respect to the scattering plane. Figures 3(c) and 3(d) display spectra for $q_{||}$ oriented parallel and perpendicular to the steps as red squares and blue circles. Parallel to the steps the spectra are as on the as-grown films on Cu(100). For wave vectors oriented perpendicular to the steps, however, the spectrum displays merely a shoulder in case of small wave vectors [Fig. 3(c)]. An extraction of the FWHM is not possible in that case. A further analysis however shows that the data are not consistent with the assumption of an unperturbed spectrum merely riding on a higher background tail of the elastic peak.

For $q_{||} = 6$ nm^{-1} [Fig. 3(d)] the tail of the elastic peaks play no role. The spectrum obtained for the wave vector oriented

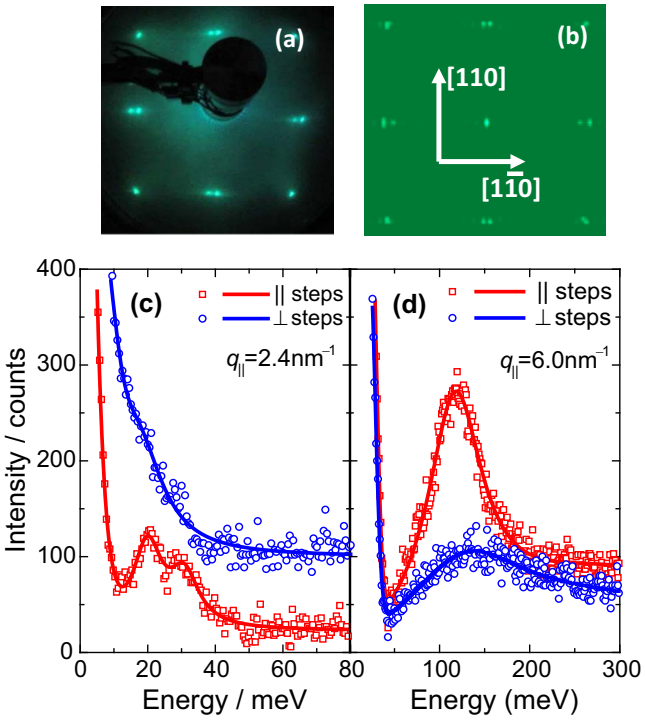

FIG. 3. LEED pattern of the 8 ML cobalt film on Cu(1 1 23) and its simulation [(a) and (b), respectively]. (c) and (d) Spectra of spin waves traveling parallel and perpendicular to the steps of the (1 1 23) cobalt film are denoted by red squares and blue circles, respectively. Spectra in (c) are vertically shifted with respect to each other. The resolution in (c) and (d) is 3.5 and 6 meV, respectively.

parallel to the steps FWHM is approximately as observed previously on flat cobalt films [8,27]. Perpendicular to the steps the spectrum is merely a broad hump. We note that qualitatively the same results are obtained for other wave vectors and on (1 1 13) films (higher step density).

A quantitative analysis of the data in Fig. 3 is not meaningful without complete theoretical understanding of the mode spectrum on stepped surfaces. Even on flat cobalt films the spin wave response at $q_{||} = 6\,\mathrm{nm}^{-1}$ involves more than a single mode [13] (primarily the lowest standing mode [22]). It is furthermore not possible to prepare films with regular array of steps of much larger distance since the stabilizing step-step repulsive interaction decays as the inverse square of the distance between steps [28]. Nevertheless, one can safely conclude from the experiments on stepped surfaces that primarily steps crossing the path of the spin waves lead to an increase of the FWHM, hence a shortening of the lifetime of the spin waves.

III. QUANTITATIVE ANALYSIS OF EXPERIMENTAL DATA

For an understanding of the experimental results in terms of a theoretical description we need to extract the true intrinsic FWHM of the spin waves. The spin wave spectral function at a particular wave vector $q_{||}$ is represented by a Lorentzian of the form

$$S(\hbar\omega) = \frac{\Gamma^2}{[\hbar\omega_0(q_{||}) - \hbar\omega]^2 + \Gamma^2}. \tag{2}$$

The spectrometer convolutes this Lorentzian with the wave vector resolution functions which are Gaussians in the $q_{||}$ direction (x direction) and perpendicular to the scattering plane (y direction). To facilitate this convolution we make use of the fact that the dispersion is approximately quadratic in $q_{||}$.

Hence

$$\hbar\omega_0 = Dq_{||}^2 \tag{3}$$

in which D is the stiffness. The wave vector convolution therefore reads

$$G(\hbar\omega) = \int dq_x dq_y e^{-q_x^2/(2s_x^2)} e^{-q_y^2/(2s_y^2)} \times \Gamma^2\left\{\hbar\omega - D\left[(q_{||}+q_x)^2 + q_y^2\right] + \Gamma^2\right\}^{-1}. \tag{4}$$

The relevant effective stiffness D for each spectrum is calculated from $q_{||}$ [Eq. (1)]) and the peak energy of the spin wave signal which we identify with $\hbar\omega_0$. The calculation of the convolution (4) requires the knowledge of the variances s_x and s_y. The value for s_x is determined from the dependence of the elastic diffuse intensity as function of angle, hence as a function of $q_{||}$, immediately after measuring a series of spectra. These experimental values are different for films in their as-grown and the annealed state, smaller for the annealed state. Even for the annealed films, however, s_x was found to be about 20% higher than calculated from the angular resolution of the spectrometer which is known from electron optical calculations [23]. The variance perpendicular to the scattering plane s_y cannot be determined experimentally. By spectrometer design it is about a factor of 3 higher than s_x. The precise value has little effect on the dispersion broadening [see Eq. (4)]. For the convolution we take s_y from the electron optical calculations.

The resulting function $G(\hbar\omega)$ is convoluted with a Gaussian representing the spectrometer energy response function. The final response function is therefore

$$F(\hbar\omega) = \int d\hbar\omega'\, G(\hbar\omega') e^{-(\hbar\omega-\hbar\omega')^2/(2s_{\mathrm{el}}^2)}. \tag{5}$$

The variance s_{el} is determined by fitting the elastic line to a Gaussian. For that purpose we use a spectrum at a wave vector where the surface acoustic phonon appears as a separate gain and loss peaks (i.e., at $q_{||} = 4.5\,\mathrm{nm}^{-1}$). Those calibration spectra were recorded immediately after completing a series of spin wave spectra as function of $q_{||}$. This ensures that the measured energy and momentum broadening indeed refers to the spectra to be analyzed.

The intrinsic FWHM of the spin wave is now determined by first assuming a Lorentzian spin wave signal of narrow linewidth. The width is then gradually increased until $F(\hbar\omega)$ matches the experimental data. Figure 4 shows an example for $q_{||} = 0.197\,\mathrm{nm}^{-1}$. The genuine spectral density of the spin wave is plotted as a blue dashed line. The green dash-dotted line is the wave vector convolution $G(\hbar\omega)$ of it. The red dotted line is the convolution only with the energy resolution function. Comparison to $G(\hbar\omega)$ shows that at $q_{||} = 0.197\,\mathrm{nm}^{-1}$ momentum and energy broadening contribute about equally to the width of the complete simulation $F(\hbar\omega)$ (red solid line). The red open circles in Fig. 4 represent the experimental spectrum of the acoustic spin wave. This data are obtained

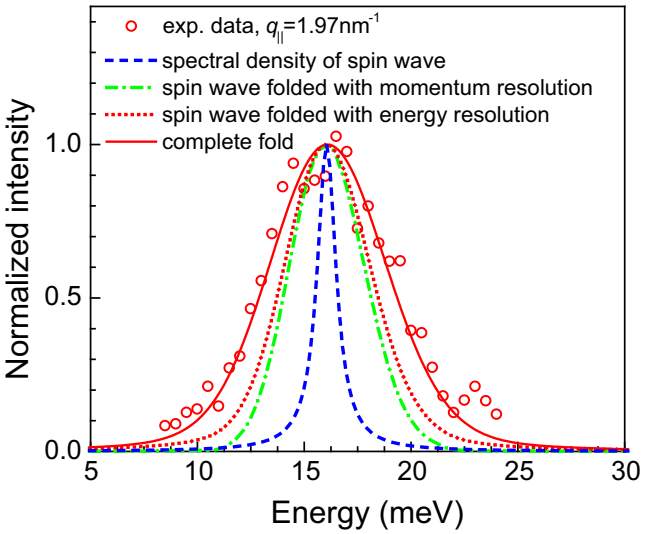

FIG. 4. See text for discussion.

as described before, namely by subtracting the tail of the elastic signal, a constant background, and a Lorentzian to fit the standing wave (Fig. 2).

Figure 5 shows the result of the unfolding process. The solid symbols are the raw FWHM before and after annealing (blue circles and red squares, respectively). These data points are the same as in Fig. 2.

The open symbols represent the FWHM after unfolding (blue open circles and red open squares, respectively). For $q_{||} < 2.2\,\mathrm{nm}^{-1}$ the error bars reach down to zero which means that even delta-function-like spin wave spectral densities would be compatible with experiment. On the other hand, intrinsic FWHM up to 2 meV are likewise compatible with experiment.

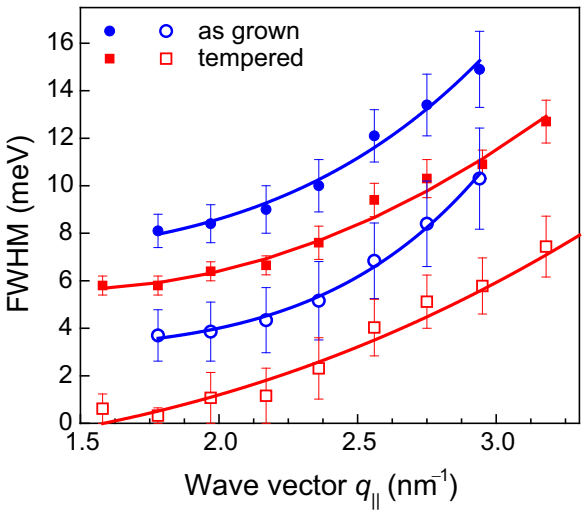

FIG. 5. The solid symbols are the raw FWHM before and after annealing (blue circles and red squares, respectively). The open symbols are the FWHM after unfolding before and after annealing (blue open circles and red open squares, respectively).

IV. THEORY

The experimental data on the spin wave dispersion and linewidth are compared to a theory for pseudomorphic flat cobalt films on Cu(100) surfaces. The theory takes fully into account the itinerant character of d states, including their hybridization with sp states [12,29]. The coupling between spin waves and Stoner excitations is thereby naturally incorporated. This allows us to determine the energies and lifetimes of spin waves without adjustable parameters.

We describe the electronic structure of pseudomorphic cobalt films on Cu(001) using a multiorbital extension of the Hubbard model, including s, p, and d states. The Slater-Koster parameters (SKP) were extracted from an *ab initio* calculation based on the real space linearized muffin tin orbital method within the atomic sphere approximation (RS-LMTO-ASA) [30–32]. Thus we are able to obtain parameters specific to the geometry of each film-substrate system considered. This is in contrast to previous calculations, for which we had to rely on SKP obtained from bulk electronic structures for Co and Cu separately [13,33]. For each film thickness we used a cluster with a number of atoms between 5500 and 9000, including the four nonequivalent Cu layers between the Co film and the bulklike remainder of the semi-infinite Cu substrate and the empty-spheres cap layer on top of the outermost Co layer. Since we determined the spin-polarized ground state within the *ab initio* part of the calculation, we need to determine the appropriate strength of the screened Coulomb interaction from the mean field transverse spin susceptibility, as described in Ref. [34]. This ensures that the Goldstone mode is obtained within the numerical precision of our calculations. We define the spin wave spectral density (SWSD) in terms of the transverse spin susceptibility matrix $\chi^{+-}_{l\mu;l'\mu'}(\hbar\Omega,\vec{q}_{||})$. l' and l are layer indices, μ' and μ are orbital indices, and $\vec{q}_{||}$ is a wave vector parallel to the film. The projection of the SWSD at atomic layer l is given by

$$S_l(\hbar\Omega;\vec{q}_{||}) \equiv -\frac{1}{\pi}\sum_{\mu'\mu\in d}\chi^{+-}_{l\mu;l'\mu'}(\hbar\Omega,\vec{q}_{||}). \qquad (6)$$

The sum over orbital indices is restricted to the d orbitals. Spin wave energies and lifetimes are extracted from our calculated spectral densities much in the same way as in experiment: We associate spin wave energies to the positions of the maxima of the spin wave spectral densities, and the lifetimes are given by the inverse of their full width at half maximum.

We chose the projection of the SWSD on the surface layer as representative of the energy loss spectrum, since the penetration depth of the electron beam is limited to a few atomic layers close to the surface and the spectral density of the acoustic wave varies little from layer to layer.

Figure 6(a) compares the calculated spin wave dispersion with experimental data for an 8 ML film (green open triangles vs blue circles and red squares for as-grown and annealed films, respectively). Quantitative agreement is found. This is in contrast to theory based on the frozen magnon concept, at least in the case of cobalt films (see, e.g., [35]). The calculated intrinsic FWHM of the spin wave peaks falls below the experimental data for larger wave vectors [Fig. 6(b), red squares]. For smaller wave vectors, however, the experimental

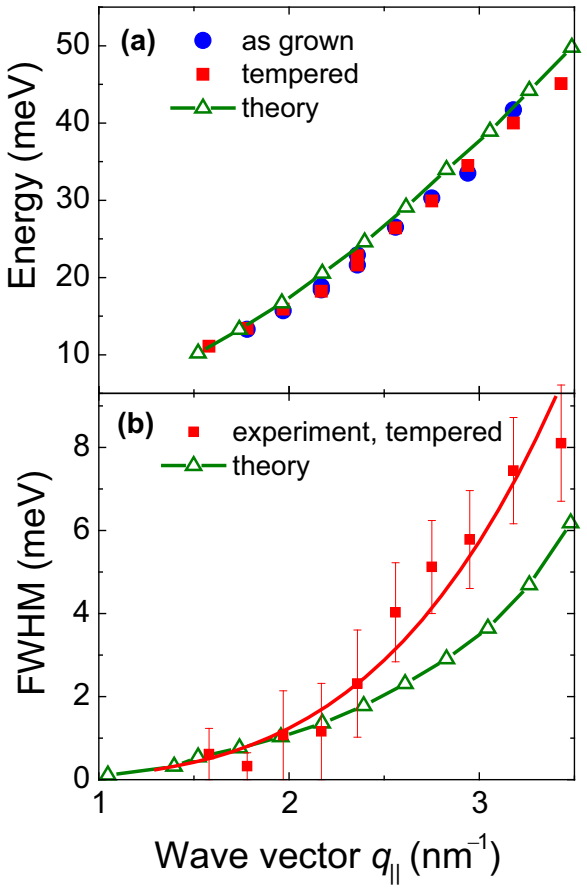

FIG. 6. (a) Experimental energies of acoustic spin waves vs $q_{||}$ for an 8 ML cobalt film in the as-grown state and after annealing are compared to theory (blue circles, red squares, and green open triangles, respectively). (b) Experimental FWHM of acoustic spin waves vs $q_{||}$ after annealing and as obtained by theory (red squares and green open triangles, respectively).

data points are consistent with theory if we take the data points by their face value. The upper limit of the error bars however falls above theory even there.

The experiment has shown that a smoothening of the surface leads to a reduction of the FWHM (Fig. 5) and that the annealed film still contains steps, albeit of lesser density (Fig. 2). It is therefore conceivable that the theoretically calculated values of the FWHM are the correct values of a perfectly flat surface in the entire wave vector range.

A possible explanation for a larger deviation of the experimental linewidth for $q_{||} \geqslant 2.5$ nm^{-1} can be derived from the fact that, starting at this this wave vector, the energies of the acoustic spin waves become similar to the energies of the first standing mode at $q_{||} \sim 0$. The steps remaining after the annealing procedure may be too few in number to disturb the acoustic mode for $q_{||} < 2.5$ nm^{-1}, but their mere existence may be enough to break the translation symmetry in the direction parallel to the film, allowing an intermixing between acoustic and standing modes of distinct wave vector and similar energies, thus reducing the lifetime of acoustic spin waves. Preliminary theoretical results obtained with a simplified model for the electronic structure in the presence of

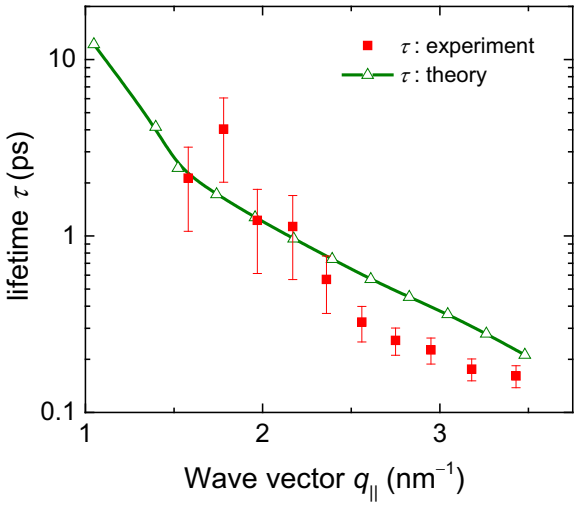

FIG. 7. Lifetimes of the acoustic spin wave in 8 ML cobalt films on Cu(100) calculated using the FWHM from Fig. 6.

a single step indicate that there is a considerable transference of spectral weight from the acoustic peak to the first standing mode in the energy range where the energies of the two modes coincide. We also find that the linewidth of the acoustic mode for wave vectors parallel to the step is unaffected by the step. Calculations based on a realistic electronic structure in the presence of an arbitrary density of steps are currently underway.

V. LIFETIME OF SPIN WAVES

For the purpose of reference to previous publications [10,11] it is useful to consider also the lifetime of the spin waves. The FWHM of a spin wave may be converted into the lifetime τ according to

$$\tau = \frac{\hbar}{\Gamma} = \frac{2\hbar}{\text{FWHM}}. \tag{7}$$

Figure 7 shows the lifetimes obtained from data on the annealed surface (red squares) and theory (open green triangles). For the smallest wave vectors the lifetimes obtained here are more than an order of magnitude larger than reported as "long living terahertz magnons" in FePd alloy films deposited on Pd(001) which were measured at $T = 13$ K [11]. Hence there is no need to search for an exotic system to realize long lifetimes of exchange-dominated spin waves in ferromagnetic metals. It suffices to go to moderately lower wave vectors. We remark further that reliable values for the lifetime of spin waves in films of more than one or two monolayer thickness can only be obtained if a particular spin wave signal can be attributed to a *single* mode. That is not the case for the 8 ML film of cobalt on Cu(100) and wave vectors larger than about 3.5 nm^{-1} [10,13,22].

VI. SURFACE STEPS AND MEAN FREE PATH OF SPIN WAVES

This section explores the hypothesis that the effect of surface steps on acoustic spin waves is that the steps limit the mean free path. This was suggested already in 1992 for the case

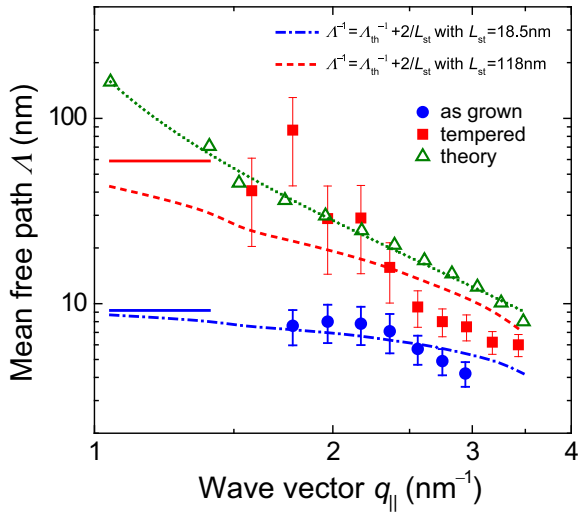

FIG. 8. Mean free paths calculated from the FWHM measured on the as-grown films, the annealed films, and from theory (solid blue circles, solid red squares, and open olive triangles, respectively). See text for discussion of the dashed and dash-dotted lines.

of magnetostatic spin waves by Stamps *et al.* [36]. The authors considered reflection and transmission of long wavelength acoustic spin waves at monatomic steps and also localized states at steps [37]. For travelling acoustic waves they showed that the boundary conditions at steps require the generation of evanescent waves at step sites. Inside the film, these evanescent waves oscillate in amplitude from layer to layer [36]. By analogy to high-momentum acoustic thin-film modes (or to high-momentum bulk spin waves) one would expect that the step-generated evanescent waves couple effectively to Stoner excitations which should cause strong damping of acoustic waves traversing the step.

The mean free path of a spin wave is the product of group velocity and lifetime

$$\Lambda = \tau \frac{\partial \omega}{\partial q_{||}}. \tag{8}$$

The lifetime in turn is obtained from the FWHM according to Eq. (7). The group velocity is calculated from the dispersion of the (acoustic) spin wave. The results for the as-grown and annealed film are shown in Fig. 8 as solid blue circles and solid red squares, respectively. The olive-green triangles are the results of theory. The olive-green dotted line is a smooth curve fitting the theoretical data.

In the following we assume that a step acts as perfect sinks for spin waves traversing the step (*sink model*). According to that model, a spin wave at the most can travel for a mean path length Λ_s of

$$\Lambda_s = \bar{L}_s/2, \tag{9}$$

where $\bar{L}_s$ is the mean distance between steps. We take mean distance between steps from the simulations of the diffuse scattering (Fig. 2). The solid blue and red lines in Fig. 8 mark the resulting upper limits. The limits are consistent with the experimental data.

One may assume further that the limitation of the mean free path by steps and by intrinsic damping on the flat portions of the film are independent processes. In that case the total mean free path Λ_{tot} should be given by

$$\Lambda_{\text{tot}}^{-1} = \Lambda_{\text{flat}}^{-1} + \Lambda_s^{-1}, \tag{10}$$

in which Λ_{flat} is the mean free path of a perfectly flat surface.

The dash-dotted blue and the dashed red line are calculated from Eq. (10) by identifying the mean free path of a perfectly flat surface Λ_{flat} with the mean free path obtained from theory and Λ_s with half the mean distance between steps [Eq. (9)].

The resulting curves follow the trend of the experimental mean free path to smaller values for larger wave vectors. The agreement is not quantitative, however. A possible reason could be that Eq. (10) is an oversimplification. A further reason could be that theory overestimates the mean free path (i.e., underestimates the FWHM) of perfectly flat surfaces at higher wave vectors.

We note further that the broadening of the spectrum observed in Fig. 3(d) for the case of spin waves traveling perpendicular to the steps on the (1 1 23) surface is consistent with the *sink model*. The distance between steps on the (1 1 23) surface, and hence the mean free path according to *sink model* is $\Lambda_s = 2.9$ nm. The step-induced additional broadening of the FWHM according the model would amount to 84 meV.

VII. CONCLUSIONS

We have shown in experiment and theory that the intrinsic lifetime and mean free path of spin waves in cobalt layers become rather large for wave vectors as small as 1.5–3 nm^{-1}. Theory predicts lifetimes in excess of 10 ps and mean free path beyond 100 nm for wave vectors of 1 nm^{-1}. Unfortunately, such low wave vectors with spin wave energies of only a few meV are not accessible at present by electron energy loss spectroscopy.

An interesting problem is posed by the question as to why steps have such a strong effect on the mean free path. The early work of Stamps *et al.* [36] only provides some hints. It is not clear inasmuch the local properties of edge atoms such as structure, magnetic moment, and exchange coupling are important. It is not implausible that a "smoothening" of the magnetic edge structure at steps by decoration with soft magnetic atoms could reduce the blocking of spin wave by steps. In that case, atomically flat surfaces would not be required for the utilization of nm spin waves in magnonic devices. To investigate those effects and to gain further insight into what actually happens when a spin wave meets a step theoretical and experimental studies of spin waves on films with regular array of steps should be helpful.

ACKNOWLEDGMENTS

The authors have benefitted from enlightening discussions with A. Ernst, S. Lounis, M. Dos Santos Dias, F. Dos Santos, and R. L. Stamps regarding spin waves. The able technical assistance of Bernd Küpper, Arnd Bremen, and Claudia Steufmehl has been instrumental to the success of this work.

[1] L. S. Robert, B. Stephan, Å. Johan *et al.*, J. Phys. D **47**, 333001 (2014).
[2] A. A. Serga, A. V. Chumak, and B. Hillebrands, J. Phys. D **43**, 264002 (2010).
[3] T. Schneider, A. A. Serga, B. Leven *et al.*, Appl. Phys. Lett. **92**, 022505 (2008).
[4] A. A. Nikitin, A. B. Ustinov, A. A. Semenov *et al.*, Appl. Phys. Lett. **106**, 102405 (2015).
[5] B. Lenk, H. Ulrichs, F. Garbs *et al.*, Phys. Rep. **507**, 107 (2011).
[6] R. Vollmer, M. Etzkorn, P. S. A. Kumar, H. Ibach, and J. Kirschner, Phys. Rev. Lett. **91**, 147201 (2003).
[7] J. Rajeswari, H. Ibach, and C. M. Schneider, Phys. Rev. Lett. **112**, 127202 (2014).
[8] J. Rajeswari, H. Ibach, C. M. Schneider, A. T. Costa, D. L. R. Santos, and D. L. Mills, Phys. Rev. B **86**, 165436 (2012).
[9] K. Zakeri, Phys. Rep. **545**, 47 (2014).
[10] Y. Zhang, T.-H. Chuang, K. Zakeri, and J. Kirschner, Phys. Rev. Lett. **109**, 087203 (2012).
[11] H. J. Qin, K. Zakeri, A. Ernst *et al.*, Nat. Commun. **6**, 6126 (2015).
[12] A. T. Costa, R. B. Muniz, and D. L. Mills, Phys. Rev. B **68**, 224435 (2003).
[13] A. T. Costa, R. B. Muniz, and D. L. Mills, Phys. Rev. B **69**, 064413 (2004).
[14] A. T. Costa, R. B. Muniz, and D. L. Mills, Phys. Rev. B **74**, 214403 (2006).
[15] P. Buczek, A. Ernst, L. Sandratskii *et al.*, J. Magn. Magn. Mater. **322**, 1396 (2010).
[16] L. M. Sandratskii and P. Buczek, Phys. Rev. B **85**, 020406 (2012).
[17] P. Buczek, A. Ernst, and L. M. Sandratskii, Phys. Rev. Lett. **106**, 157204 (2011).
[18] K. Heinz, S. Müller, and L. Hammer, J. Phys.: Condens. Matter **11**, 9437 (1999).
[19] L. Gonzalez, R. Miranda, M. Salmeron, J. A. Verges, and F. Yndurain, Phys. Rev. B **24**, 3245 (1981).
[20] H. Ibach, *Physics of Surfaces and Interfaces* (Springer, Berlin, 2006).
[21] E. Michel, H. Ibach, and C. M. Schneider, Phys. Rev. B **92**, 024407 (2015).
[22] H. Ibach, Surf. Sci. **630**, 301 (2014).
[23] H. Ibach and J. Rajeswari, J. Electron Spectrosc. Relat. Phenom. **185**, 61 (2012).
[24] H. Ibach, J. Rajeswari, and C. M. Schneider, Rev. Sci. Instrum. **82**, 123904 (2011).
[25] T. Allmers and M. Donath, Surf. Sci. **605**, 1875 (2011).
[26] M. Giesen, F. Schmitz, and H. Ibach, Surf. Sci. **336**, 269 (1995).
[27] M. Etzkorn, Thesis, Martin-Luther University Halle-Wittenberg, 2005, urn:nbnde:gbv:3-000008590.
[28] N. C. Bartelt, T. L. Einstein, and E. D. Williams, Surf. Sci. **240**, L591 (1990).
[29] A. T. Costa, R. B. Muniz, S. Lounis, A. B. Klautau, and D. L. Mills, Phys. Rev. B **82**, 014428 (2010).
[30] P. R. Peduto, S. Frota-Pessoa, and M. S. Methfessel, Phys. Rev. B **44**, 13283 (1991).
[31] O. K. Andersen, Phys. Rev. B **12**, 3060 (1975).
[32] O. K. Andersen and O. Jepsen, Phys. Rev. Lett. **53**, 2571 (1984).
[33] A. T. Costa, R. B. Muniz, and D. L. Mills, Phys. Rev. B **70**, 054406 (2004).
[34] S. Lounis, A. T. Costa, R. B. Muniz, and D. L. Mills, Phys. Rev. B **83**, 035109 (2011).
[35] L. Bergqvist, A. Taroni, A. Bergman, C. Etz, and O. Eriksson, Phys. Rev. B **87**, 144401 (2013).
[36] R. L. Stamps, R. E. Camley, B. Hillebrands, and G. Guntherodt, Phys. Rev. B **46**, 10836 (1992).
[37] R. L. Stamps, R. E. Camley, B. Hillebrands, and G. Guntherodt, Phys. Rev. B **47**, 5072 (1993).